Criteria for static equilibrium in particulate mechanics computations

Xuxin Tu[*], José E. Andrade

Department of Civil and Environmental Engineering, Northwestern University,

Evanston, IL 60208, USA

Abstract

The underlying physics of granular matter can be clearly solved using particulate mechanics methods, e.g., the discrete element method (DEM) that is inherently discontinuous and heterogeneous. To solve static problems, explicit schemes using dynamic relaxation procedures have been widely employed, in which naturally dynamic material parameters are typically adapted into pure numerical artifacts with the sole purpose of attaining meaningful results. In discrete computations using these explicit schemes, algorithmic calibration is demanded under general conditions in order to achieve quasi-static states. Until now, procedures for algorithmic calibration have remained rather heuristic. This paper presents two criteria, using the concept of homogenized stresses, for evaluating equilibrium in quasi-static applications of particulate mechanics methods. It is shown, by way of numerical examples, that the criteria for static equilibrium can be applied successfully to obtain quasi-static solutions in explicit DEM codes through algorithmic calibrations. A general procedure is proposed herein for carrying out the algorithmic calibration effectively and efficiently.

Keywords

---

[*]Corresponding author. E-mail: x-tu@northwestern.edu

1 Introduction

Granular materials are ubiquitous in nature and in industry. In nature, granular materials abound as they constitute the fundamental ingredients of many geomaterials, including soils, rocks, and concrete. In industry, granular materials populate products in the pharmaceutical, chemical, mining, agricultural, and food industries. Problems typically involve understanding the mechanical behavior of such complex systems. In engineering, extraction of stress-strain laws in these materials is of crucial importance for the understanding, modeling, and prediction of engineering products. From a modeling standpoint, the finite element method constitutes perhaps the most powerful and versatile tool for modeling engineering systems, including granular media. However, it is clear that the behavior of granular systems is encoded at the particle scale, propagating all the way to the macroscopic scale.

In an effort to develop the discrete mechanics for granular matter, Cundall and Strack [1] proposed the discrete element method (DEM) in the late seventies. In DEM, rigid particles are governed by Newtonian dynamics and are allowed to interact with each other by contact. Due to its versatility, DEM has become an important tool in investigating micro-scale mechanisms in granular materials [2; 3]. The method has captured the attention of many researchers and has been used to model a plethora of materials such as rocks [4], asphalt mixtures [5], concrete [6], and clays [7]. Industrial applications include modeling of chemical particles [8], powders [9] and nanoparticles [10]. The method has also been used to investigate the effect of shape (especially on the dilatancy properties of granular materials) including polyhedral blocks [11], ellipsoids [12], and arbitrary shapes using overlapping rigid clusters [13]. Engineering applications of the method include penetration of concrete targets [14], generation of constitutive relations for granular materials [15; 16], investigation of the microscopic mechanism of shear banding [17], and simulation of fluidized beds, widely used in chemical and industrial applications [8].

Perhaps, as pointed out by Ng [18], the beauty of DEM is its simplicity. However, in many of the aforementioned applications (including in the pioneering work of Cundall and Strack [1]) Newton's equations are used to simulate steady-state or quasi-static conditions

where inertia terms typically vanish. Occasionally, input algorithmic parameters that belong to dynamic simulations (e.g., damping, fictitious mass) are assigned values without any physical or mathematical justification, in some instances with the sole purpose of attaining a steady-state solution. One could argue that computational expense and spurious parameter calibration have prevented the method from penetrating practice further. In the case of computational expense, it is expected that full-scale computations using DEM will be possible in the next twenty years [19] and steps to accelerate that rate using multi-scale techniques and hybrid approaches are already underway (see the works in [20] and [21]). The issue related to parameter calibration is still unresolved and furnishes the motivation for this paper.

To solve static problems (omnipresent in engineering) using explicit schemes, 'dynamic relaxation' procedures have been typically employed [22]. These procedures are based on the fundamental idea, originally proposed by Rayleigh [23], that the static solution of a mechanical system can be viewed as the steady-state part of a corresponding dynamic problem. This method was widely applied to finite difference and finite element methods especially in non-linear structural analysis [24–26], and various algorithms were developed to automatically adjust the algorithmic parameters [22; 27; 28]. Based on the conditions for optimal convergence of dynamic relaxation [22] and the properties of the Rayleigh quotient, Bardet and Proubet [29] proposed an adaptive algorithm for explicit discrete element methods, which has demonstrated its success in randomly-packed assemblies. In contrast to a numerical method used for continuum materials, however, the discrete element method encounters more variations and uncertainties in simulating an arbitrary granular system. Variations in particle geometry, particle size distribution, contact law, contact forming and breaking, etc., are difficult to take into account in an adaptive algorithm for automatic parameter update. As a result, algorithmic calibration, i.e., choosing values for the algorithmic parameters involved in explicit DEM schemes, is generally required to perform quasi-static simulations. The crux of the problem is the evaluation of static equilibrium in explicit DEM computations in the context of quasi-static applications.

In this paper, criteria for the evaluation of static equilibrium are derived using a rather

general approach. It is shown that these criteria boil down to conservation of linear and angular momenta in the 'homogenized' problem, following lines close to those proposed by Christoffersen et al [30]. A general assembly of particles is forced to obey static equilibrium, which will in turn imply conditions on the homogenized stress tensor. Even though the conservation of momenta of the homogenized problem is not particularly new, the idea of utilizing the implied qualities of the homogenized stress as necessary macroscopic criteria for static equilibrium is novel. A further innovation in this paper is the use of the criteria to systematically calibrate explicit DEM codes to achieve quasi-static states under general conditions. In doing so, this paper contributes to the unresolved issue of parameter calibration by proposing a framework bolstered by conditions of static equilibrium from the onset of computation. We generalize our findings and outline a procedure for consistent algorithmic calibration in DEM.

The organization of the paper is as follows. First, the most widely used explicit scheme for DEM simulations and its algorithmic calibration is briefly described to illustrate the potential issues arising in the numerical solution. Second, the necessary criteria for static equilibrium in an arbitrary granular assembly are presented. Then, these criteria are used to calibrate a 'benchmark' example where parametric studies are performed to show the effects of deviating from the 'optimal' parameters. Finally, a general procedure for calibration of explicit DEM codes for quasi-static applications is presented and some conclusions based on our findings are drawn.

As for notations and symbols used in this paper, bold-faced letters denote tensors and vectors; the symbol '·' denotes an inner product of two vectors (e.g. $\boldsymbol{a} \cdot \boldsymbol{b} = a_i b_i$), or a single contraction of adjacent indices of two tensors (e.g. $\boldsymbol{c} \cdot \boldsymbol{d} = c_{ij} d_{jk}$); the symbol '⊗' denotes a juxtaposition, e.g., $(\boldsymbol{a} \otimes \boldsymbol{b})_{ij} = a_i b_j$ and the symbol '×' denotes a cross product between two vectors, e.g., $(\boldsymbol{a} \times \boldsymbol{b})_k = \epsilon_{ijk} a_i b_j$, where ϵ_{ijk} is the permutation operator.

2 DEM schemes and algorithmic calibration

As mentioned in the introduction, DEM codes are often used to model quasi-static engineering problems. However, to achieve quasi-static states in explicit DEM schemes, the algorithmic parameters involved must be properly calibrated, a procedure typically referred to as *algorithmic calibration*. Without algorithmic calibration, the explicit method tends to yield erroneous results and thus becomes useless. Unfortunately, algorithmic calibration is generally ignored in practice and the involved parameters are often assigned on an arbitrary basis, which has made it difficult to compare results from different sources and could undermine the scientific value of the reported data. Therefore, it is crucial to regularize the algorithmic calibration for the explicit DEM scheme.

To this end, there are two fundamental questions to be answered. First, what criteria should be used to effectively evaluate convergence of the numerical scheme to quasi-static equilibrium? In particulate mechanics methods, it is always possible to evaluate equilibrium for each individual particle. However, it is not desirable to evaluate the balance of a system directly based on individual evaluations. Sometimes, the overall kinetic energy is employed to judge if a granular system reaches quasi-static states. Nevertheless, zero kinetic energy does not necessarily infer quasi-static equilibrium. The second fundamental question is: what procedure should one follow to perform the algorithmic calibration? These two questions are interconnected; one can use the criteria both to consistently enforce static equilibrium and to systematically calibrate explicit DEM schemes for static applications.

In order to begin answering the aforementioned questions, it is first necessary to understand the underlying methodology used in explicit DEM codes and their intimate dependence on the algorithmic parameters used. The subsequent sections outline some of these issues.

2.1 Particle interactions and governing equations

In DEM, interparticle interactions are typically treated in normal and tangential components at contact points. In the normal direction, the normal force f_n is related to the normal

displacement δ_n such that

$$f_n = k_n \delta_n \tag{2.1}$$

where k_n is the normal contact stiffness. To obtain more realistic results, Herzian normal contact law [31] is usually employed, with k_n expressed as

$$k_n = \frac{E_\mu \sqrt{2r\delta_n}}{3(1 - \nu_\mu^2)} \tag{2.2}$$

where r is the radius of particle, E_μ is the Young's modulus and ν_μ is the Poisson's ratio of the particles. In this work, only elastic normal contact is considered. In the tangential direction, the tangential force f_t is related to the tangential displacement δ_t. Using the Coulomb frictional law, a general expression for a tangential contact model reads

$$f_t = \min(k_t |\delta_t|, \tan \phi_\mu f_n) \frac{\delta_t}{|\delta_t|} \tag{2.3}$$

where k_t is the tangential contact stiffness and ϕ_μ is the intergranular friction angle. According to Mindlin and Deresiewicz [32], k_t is related to k_n via

$$k_t = \frac{3(1 - \nu_\mu)}{2 - \nu_\mu} k_n \tag{2.4}$$

In light of the force-displacement laws outlined above, each contact can be idealized as two springs in the normal and tangential directions, as shown in Figure 1. By perturbing an individual particle while fixing its neighboring particles, the governing equation for this particle—in static equilibrium—can be expressed as

$$\boldsymbol{K}^p \cdot \boldsymbol{u}^p = \boldsymbol{f}^p \tag{2.5}$$

where $\boldsymbol{K}^p$, the *local* stiffness matrix, assembles the stiffness contribution from each contact on the particle, while $\boldsymbol{u}^p$ and $\boldsymbol{f}^p$ are the generalized displacement vector and force vector, respectively. The dimension of $\boldsymbol{u}^p$, or $\boldsymbol{f}^p$, corresponds to the number of degrees of freedom

(DOF), denoted by N_{dof}. For a 2D problem, $N_{\mathrm{dof}} = 3$, corresponding to two translation DOFs and one rotation DOF. Hence the term 'generalized' is used for naming $\boldsymbol{u}^{\mathrm{p}}$ and $\boldsymbol{f}^{\mathrm{p}}$. For a translation DOF, the corresponding component of $\boldsymbol{f}^{\mathrm{p}}$ is a measure of force. On the other hand, for a rotation DOF, it is a measure of moment. For a nonlinear relation, such as the Herzian contact law, $\boldsymbol{K}^{\mathrm{p}}$ is a function of k_{n}, k_{t} and ϕ_{μ} at each contact point. Therefore, $\boldsymbol{K}^{\mathrm{p}}$ is dependent on the particle displacement $\boldsymbol{u}$ and equation (2.5) represents a generally nonlinear relation. An example of how to construct the local stiffness matrix can be found in the work of van Baars [33].
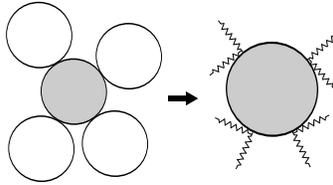
Figure 1: Equivalent mass-spring system for an individual particle within a granular system.

Assembling equation (2.5) over all particles in the granular system yields

$$\boldsymbol{K} \cdot \boldsymbol{u} = \boldsymbol{f}^{\mathrm{ext}} \tag{2.6}$$

where $\boldsymbol{K}$ is the *global* stiffness matrix with dimensions $(N_{\mathrm{p}} \times N_{\mathrm{dof}}) \times (N_{\mathrm{p}} \times N_{\mathrm{dof}})$ with N_{p} as the total number of particles in the system, $\boldsymbol{u}$ is the global displacement vector, and $\boldsymbol{f}^{\mathrm{ext}}$ is the external force vector—the counterpart of the internal force vector $\boldsymbol{f}^{\mathrm{int}}$, which is equal to the left hand side of equation (2.6). The global entities in equation (2.6) are assembled from their local counterparts $\boldsymbol{K}^{\mathrm{p}}$, $\boldsymbol{u}^{\mathrm{p}}$ and $\boldsymbol{f}^{\mathrm{p}}$ in a procedure similar to that followed in FEM to obtain global arrays based on local arrays [34; 35]. Effectively, equation (2.6) defines the governing equation for any granular system under static equilibrium, which often is simply expressed as

$$\boldsymbol{f}^{\mathrm{tot}} = \boldsymbol{f}^{\mathrm{ext}} - \boldsymbol{f}^{\mathrm{int}} = \boldsymbol{0} \tag{2.7}$$

prescribed loads/deformations $\Rightarrow f_n^{\text{ext}}$

$n = n+1$
$f_n^{\text{int}} = f_k^{\text{int}}$

$k = 0$
$f_k^{\text{tot}} = f_n^{\text{ext}} - f_n^{\text{int}}$

Y $\quad \|f_k^{\text{tot}}\| < TOL$? $\leftarrow$ $k = k+1$

Stage 1 N

$\ddot{u}_{k+1} = M^{-1} \cdot (f_k^{\text{tot}} - D \cdot \dot{u}_k)$
$\dot{u}_{k+1} = \ddot{u}_{k+1}\Delta t$
$\Delta u_{k+1} = \dot{u}_{k+1}\Delta t$

Stage 2

$u_{k+1} = u_k + \Delta u_{k+1}$
$f_{k+1}^{\text{int}} = K_{k+1} \cdot u_{k+1}$
$f_{k+1}^{\text{tot}} = f_{k+1}^{\text{ext}} - f_{k+1}^{\text{int}}$

(a)

prescribed loads/deformations $\Rightarrow f_n^{\text{ext}}$

$f_n^{\text{tot}} = f_n^{\text{ext}} - f_n^{\text{int}}$

$n = n+1$

Stage 1

$\ddot{u}_{n+1} = M^{-1} \cdot (f_n^{\text{tot}} - D \cdot \dot{u}_n)$
$\dot{u}_{n+1} = \ddot{u}_{n+1}\Delta t$
$\Delta u_{n+1} = \dot{u}_{n+1}\Delta t$

Stage 2

$u_{n+1} = u_n + \Delta u_{n+1}$
$f_{n+1}^{\text{int}} = K_{n+1} \cdot u_{n+1}$

(b)
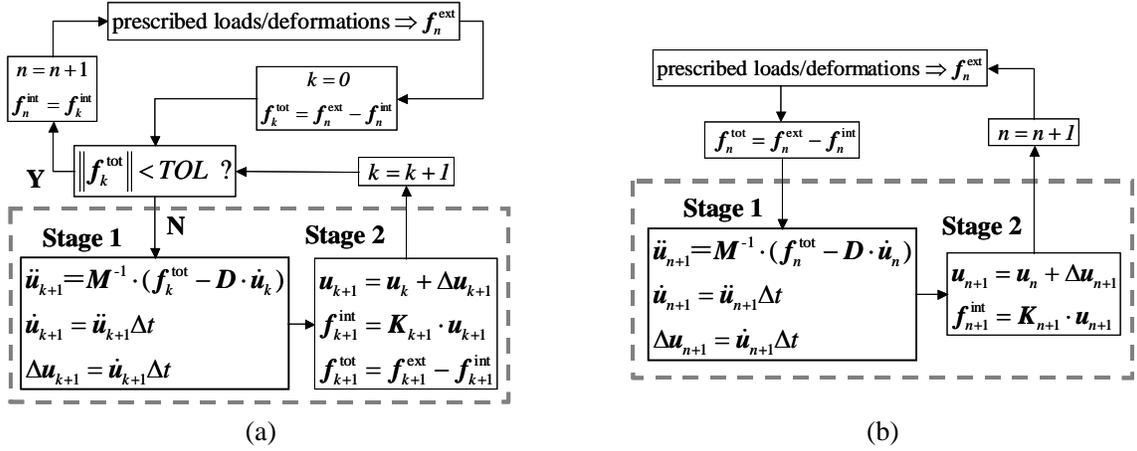
Figure 2: Flowcharts of two typical explicit schemes for static DEM: (a) iterative scheme, and (b) stationary scheme.

2.2 Motion equations and explicit schemes

Equations (2.6) and (2.7) bear a great resemblance to the matrix form of static FEM and can be solved using an implicit scheme [33]. In practice, however, explicit schemes using dynmaic relaxation procedures [22] are greatly preferred for solving DEM systems, due to their simplicity and claimed computational inexpensiveness [36].

Figure 2 shows two prototypical explicit schemes used for static DEM, with the first being iterative and the second being stationary. In either scheme, the overall progress is controlled by prescribed loads or displacements, which are added incrementally. The subscript n denotes the step number (used in both schemes) while the subscript k indicates the iteration number (used only in the iterative scheme). From Figure 2, it can be seen that the cores of these two schemes, outlined by the dashed lines, consist of two stages and are quite similar to each other. For the iterative scheme, the first stage employs the following set of motion equations with damping to compute Δu, the correction to the particle displacement, given f_k^{tot}, the unbalanced force resulting from the last iteration,

$$\ddot{u}_{k+1} = M^{-1} \cdot \left(f_k^{\text{tot}} - D \cdot \dot{u}_k\right); \quad \dot{u}_{k+1} = \ddot{u}_{k+1}\Delta t; \quad \Delta u_{k+1} = \dot{u}_{k+1}\Delta t \qquad (2.8)$$

where $\ddot{u}$ and $\dot{u}$ are the generalized acceleration and velocity, respectively; M is the mass

matrix containing the fictitious mass [29] for each particle; $\boldsymbol{D}$ is the damping matrix composed of damping coefficients for each particle in each DOF and Δt is the time step. In the second stage, shown in Figure 2a, the displacement vector $\boldsymbol{u}$ is updated. Then, the contact stiffness $\boldsymbol{K}$ and the internal force vector $\boldsymbol{f}^{\mathrm{int}}$ are updated based on the new value of $\boldsymbol{u}$. Subsequently, the total force vector $\boldsymbol{f}^{\mathrm{tot}}$ is reevaluated. This two-stage procedure is repeated until the total or unbalanced force $\boldsymbol{f}^{\mathrm{tot}}$ is dissipated, i.e., $\|\boldsymbol{f}^{\mathrm{tot}}\|$ is less than a small number, typically assigned in an arbitrary manner. Note that the stiffness matrix $\boldsymbol{K}$ is not actually assembled in explicit DEM schemes. It is used here for a concise mathematical presentation since updating every individual contact stiffness is equivalent to updating the overall stiffness.

The stationary scheme differs from the iterative scheme in two main aspects. First, the two-stage procedure in the former scheme is invoked only once for each increment of prescribed boundary conditions. Second, the magnitude of the increment in the stationary scheme is generally much smaller than that in the iterative scheme. Despite the differences, both schemes aim to achieve quasi-static states. Their relation is analogous to that between a stepwise consolidation test and a gradual consolidation test in soil mechanics. In the former test, vertical loads are added in finite steps and a relatively long period of time is placed between consecutive steps to allow excess pore pressure to dissipate. In the latter case, loads are gradually increased at a slow rate, which can be regarded as using a large number of small steps to exert the same amount of total load within the same period of time. In the numerical schemes, the counterpart of the excess pore pressure is the kinetic energy introduced by the procedure of dynamic relaxation.

In fact, the stationary explicit scheme for static DEM is form-identical to an explicit scheme for dynamic DEM, which solves the following governing equation,

$$\boldsymbol{M} \cdot \ddot{\boldsymbol{u}} + \boldsymbol{D} \cdot \dot{\boldsymbol{u}} + \boldsymbol{K} \cdot \boldsymbol{u} = \boldsymbol{f}^{\mathrm{ext}} \tag{2.9}$$

To solve this dynamic problem, the scheme depicted in Figure 2b can be used. Nevertheless, these two schemes are fundamentally different. The scheme for dynamic DEM faithfully describes the physics of particles under dynamic conditions. Therefore, the parameters involved

therein must truly represent the real material properties. For instance, the damping $\boldsymbol{D}$ should be ideally measured from relevant experiments. In contrast, most parameters involved in the *static* DEM scheme, including $\boldsymbol{M}$, $\boldsymbol{D}$, Δt, etc., serve as pure numerical artifacts and generally have no relation to their physical counterparts. For instance, the fictitious mass is often up-scaled by orders of magnitude in static DEM to reduce dynamic effects [37]. Their values are assigned with the sole purpose of achieving quasi-static states, i.e., dissipating kinetic energy while balancing external forces throughout the particulate system.

2.3 Algorithmic calibration

From the previous discussions, it becomes clear that equation (2.6) is the governing equation to be solved in any static problem, while equation (2.9) represents the dynamic relaxation procedure employed by explicit schemes to converge to the governing equation. However, the dynamic relaxation does not necessarily guarantee that equation (2.6) can be recovered. In fact, it is easy to obtain erroneous results using explicit DEM schemes, if the involved algorithmic parameters are simply assigned on an arbitrary basis.

According to equation (2.8), the displacement correction algorithm used in explicit schemes essentially is given by the following relation,

$$\Delta \boldsymbol{u}_{k+1} = \boldsymbol{M}^{-1} \cdot \left(\boldsymbol{f}_k^{\text{tot}} - \boldsymbol{D} \cdot \dot{\boldsymbol{u}}_k \right) (\Delta t)^2 \tag{2.10}$$

Hence, this algorithm is affected by the chosen algorithmic parameters: the fictitious mass $\boldsymbol{M}$, the damping $\boldsymbol{D}$ and the time step Δt. Their effects on the quality of solution are best illustrated in a 1-DOF system under 1-D conditions. As shown in Figure 3, m, D, u and f represent the scalar counterparts of $\boldsymbol{M}$, $\boldsymbol{D}$, $\boldsymbol{u}$ and $\boldsymbol{f}$, respectively. The bold curves indicate the relation between the static total force and the particle displacement, which is governed by contact stiffness. The quasi-static solution u^* corresponds to certain external force prescribed on the system. As shown in Figure 3a, if the value of D is not assigned appropriately, $D\dot{u}$ might exceed f^{tot}. As a result, Δu will diverge from the quasi-static solution u^* during the dynamic relaxation. Even if the displacement is updated in the right direction, as shown in

10

Figure 3b, wherein $(f^{\text{tot}} - D\dot{u})$ is positive, improper assignment of the algorithmic parameters could lead to an extremely slow update rate, effectively rendering the method useless. For example, if $(f^{\text{tot}} - D\dot{u})$ is relatively small or $(\Delta t)^2/m$ is relatively large, a slow convergence rate can be expected. In a stationary explicit scheme, note that u^* will evolve as the external load increases. With inappropriate parameters, the displacement update might keep lagging behind load increments, and quasi-static states might never be achieved. In fact, the loading rate, indicating how 'fast' the boundary conditions are applied, is another algorithmic parameter that affects the quality of the explicit scheme for solving static problems, and it will be discussed later.
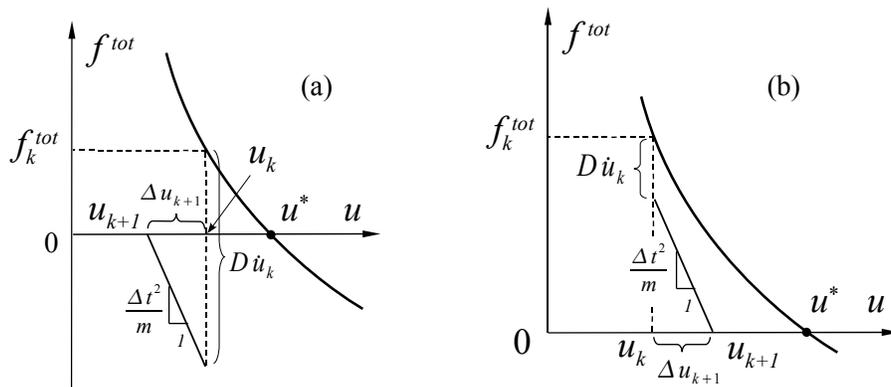
Figure 3: Two scenarios for displacement update using dynamic relaxation: (a) update away from static equilibrium; (b) update toward static equilibrium.

Therefore, it is clear that if the algorithmic parameters used in explicit DEM, such as damping, fictitious mass, time step and loading rate, are not calibrated appropriately for the quasi-static range, the numerical solutions obtained will be erroneous. Unfortunately, there was no general procedure available to quantify static equilibrium and to calibrate algorithmic parameters for the quasi-static regime. The following sections outline a very promising framework to answer the two questions posed at the beginning, i.e., what criteria should be used to evaluate the quasi-static state in the explicit scheme, and how should the calibration be performed using these criteria. It turns out that appropriate criteria to enforce static equilibrium in an assembly of grains can be systematically utilized to calibrate algorithmic parameters in explicit DEM codes.

11
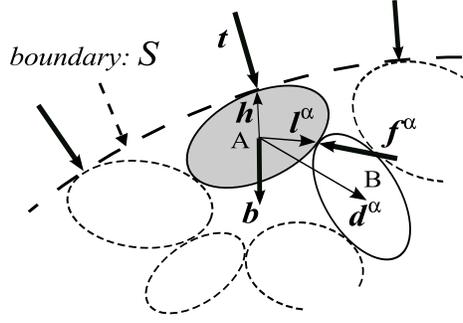
Figure 4: Internal and external forces on particles.

Remark 1. The algorithmic calibration discussed in this paper should be distinguished from the material calibration procedure commonly used in DEM simulations, in which the material parameters (e.g., E_μ, ν_μ, ϕ_μ, etc.) are adjusted so that computed responses match experimental observations.

3   Criteria for static equilibrium

For an individual particle within a granular assembly subjected to external tractions and body forces, the balance of linear and angular momenta necessitates,

$$\sum_{\alpha=1}^{n_c} \boldsymbol{f}^\alpha + \boldsymbol{t} + \boldsymbol{b} = 0$$
$$\sum_{\alpha=1}^{n_c} \boldsymbol{l}^\alpha \times \boldsymbol{f}^\alpha + \boldsymbol{h} \times \boldsymbol{t} = \boldsymbol{0} \tag{3.1}$$

where n_c is the total number of contacts acting on the particle, and the superscript α denotes the αth contact. As illustrated in Figure 4, $\boldsymbol{f}^\alpha$ is the contact force at contact α, which is an internal force, $\boldsymbol{t}$ is the external force acting on the boundary, $\boldsymbol{b}$ is the body force, $\boldsymbol{l}^\alpha$ is the distance vector emanating from the centroid of the particle to the contact point α, and $\boldsymbol{h}$ is the distance vector emanating from the centroid of the particle to the point where $\boldsymbol{t}$ is exerted.

12

Summing equation (3.1) over all particles yields,

$$\sum_{\beta=1}^{N_{\mathrm{t}}} \boldsymbol{t}^{\beta} + \sum_{p=1}^{N_{\mathrm{p}}} \boldsymbol{b}^{p} = \boldsymbol{0}$$
$$\sum_{\beta=1}^{N_{\mathrm{t}}} \boldsymbol{h}^{\beta} \times \boldsymbol{t}^{\beta} + \sum_{p=1}^{N_{\mathrm{p}}} \sum_{\alpha=1}^{n_{c}} \boldsymbol{l}^{p\alpha} \times \boldsymbol{f}^{p\alpha} = \boldsymbol{0}$$

(3.2)

where N_{p} is the total number of particles, and N_{t} is the total number of external forces imposed on the boundary. Note that both $\boldsymbol{l}$ and $\boldsymbol{h}$ are reckoned with respect to the centroids of the corresponding particles. Equation (3.2) designates the conditions for static force and static moment balances. However, equation (3.2) does not serve as a desirable criterion, because the force measures therein depend on the size of the assembly and thus they do not represent average mechanical states of the assembly.

3.1 Homogenized stress and external stress

To describe the stress state of a particulate assembly, an average stress tensor, herein referred to as the *homogenized stress*, has been derived and has been frequently used in the micromechanics of granular materials [30; 38–40]. However, its properties related to static equilibrium have not been clearly pointed out and thus have not been fully utilized. It will be shown that the most important qualities of the homogenized stress can be used as criteria to evaluate static equilibrium. These properties are inferred from the mathematical derivation of the homogenized stress, starting from the application of the principle of virtual work to the internal and external forces in static balance:

$$\sum_{\alpha=1}^{N_c} \boldsymbol{f}^{\alpha} \cdot \boldsymbol{\Delta}^{\alpha} + \sum_{\beta=1}^{N_t} \boldsymbol{t}^{\beta} \cdot \boldsymbol{u}^{\beta} + \sum_{p=1}^{N_p} \boldsymbol{b}^{p} \cdot \boldsymbol{u}^{p} = 0$$

(3.3)

where $\boldsymbol{\Delta}^{\alpha}$ is the virtual displacement at contact α; $\boldsymbol{u}^{\beta}$ is the virtual displacement at the point β where the traction $\boldsymbol{t}^{\beta}$ is applied; $\boldsymbol{u}^{p}$ is the virtual displacement at the particle centroid and N_c, N_t and N_p are the total numbers of contacts, boundary forces and particles, respectively.

As shown in Figure 4, the particulate system can be enveloped by a smooth surface S, on which it is always possible to replace the boundary force $\boldsymbol{t}$ with some equivalent traction

$\boldsymbol{T}$, as typically done in continuum mechanics. Similarly, the body force $\boldsymbol{b}$ can be replaced by some equivalent force density $\boldsymbol{B}$ for a continuum entity mechanically equivalent to the particulate system. Therefore,

$$\sum_{\alpha=1}^{N_c} \boldsymbol{f}^\alpha \cdot \boldsymbol{\Delta}^\alpha + \int_S \boldsymbol{T} \cdot \boldsymbol{u} \, dS + \int_V \boldsymbol{B} \cdot \boldsymbol{u} \, dV = 0 \tag{3.4}$$

where V is enclosed by S. Suppose the virtual displacement field $\boldsymbol{u}$ is a linear function of the particle position $\boldsymbol{x}$,

$$\boldsymbol{u} = \boldsymbol{\phi} \cdot \boldsymbol{x} + \boldsymbol{c} \tag{3.5}$$

where the tensor $\boldsymbol{\phi}$ and the vector $\boldsymbol{c}$ are arbitrary and constant, while the particle coordinates $\boldsymbol{x}$ are evaluated at the centroid of the particle. For two particles A and B in contact at point α, the virtual displacement $\boldsymbol{\Delta}^\alpha$ can be computed as follows,

$$\boldsymbol{\Delta}^\alpha = \boldsymbol{u}^A - \boldsymbol{u}^B = -\boldsymbol{\phi} \cdot \boldsymbol{d}^\alpha \tag{3.6}$$

where $\boldsymbol{u}^A$ and $\boldsymbol{u}^B$ are virtual displacements of the two particles, the contact force $\boldsymbol{f}^\alpha$ equals the force applied on particle A, and $\boldsymbol{d}^\alpha$ is the vector emanating from the centroid of A to the centroid of B, as illustrated in Figure 4. Substituting equations (3.5) and (3.6) into (3.4), and invoking the divergence theorem and the condition of static equilibrium, it can be shown that

$$-\sum_{\alpha=1}^{N_c} \boldsymbol{f}^\alpha \otimes \boldsymbol{d}^\alpha + \int_V \boldsymbol{\sigma} \, dV = 0 \tag{3.7}$$

where $\boldsymbol{\sigma}$ is the local stress tensor for the equivalent continuum domain. Consequently, the homogenized stress tensor is obtained, i.e.,

$$\bar{\boldsymbol{\sigma}} = \frac{1}{V} \sum_{\alpha=1}^{N_c} \boldsymbol{f}^\alpha \otimes \boldsymbol{d}^\alpha \tag{3.8}$$

This homogenized stress has two important properties related to linear and angular momenta, described in Sections 3.2 and 3.3 below.

3.2 Balance of linear momentum

By substituting equations. (3.5) and (3.6) into (3.3), it can be shown that

$$\frac{1}{V} \sum_{\alpha=1}^{N_c} \boldsymbol{f}^\alpha \otimes \boldsymbol{d}^\alpha = \frac{1}{V} \left(\sum_{\beta=1}^{N_t} \boldsymbol{t}^\beta \otimes \boldsymbol{x}^\beta + \sum_{p=1}^{N_p} \boldsymbol{b}^p \otimes \boldsymbol{x}^p \right) \tag{3.9}$$

Both $\boldsymbol{x}^\beta$ and $\boldsymbol{x}^p$ are position vectors locating the centroid of a particle, while $\boldsymbol{x}^\beta$ specifically refers to the particle on which $\boldsymbol{t}^\beta$ is applied. The right hand side of equation (3.9) is defined here as the *external stress*,

$$\bar{\boldsymbol{e}} = \frac{1}{V} \left(\sum_{\beta=1}^{N_t} \boldsymbol{t}^\beta \otimes \boldsymbol{x}^\beta + \sum_{p=1}^{N_p} \boldsymbol{b}^p \otimes \boldsymbol{x}^p \right) \tag{3.10}$$

Using the definition given in equation (3.8), one concludes that

$$\boxed{\bar{\boldsymbol{\sigma}} = \bar{\boldsymbol{e}}} \tag{3.11}$$

In essence, the homogenized stress represents an average of internal forces, while the external stress represents an average of external forces. When the body force is ignored, as is frequently done in practice, the resulting expression for the external stress becomes

$$\bar{\boldsymbol{b}} = \frac{1}{V} \sum_{\beta=1}^{N_t} \boldsymbol{t}^\beta \otimes \boldsymbol{x}^\beta \tag{3.12}$$

where $\bar{\boldsymbol{b}}$ is referred to as the *boundary stress*. Then equation (3.11) reduces to

$$\bar{\boldsymbol{\sigma}} = \bar{\boldsymbol{b}} \tag{3.13}$$

Equation (3.11), or (3.13), constitutes a reduced expression for the balance of linear momentum in a general granular assembly and serves as an alternative and partial expression for equation (2.7). The former equation only involves translation DOFs according to its derivation, while the force vectors in the latter equation are generalized, i.e., they include

15

components for both translation and rotation DOFs. The advantage of the expression in equation (3.11) is that it is independent of the size of the granular assembly. Based on the derivation shown above, equation (3.11) is a necessary condition for static equilibrium. As discussed later in Section 4.1, equation (3.11) can serve as an unambiguous criterion, if evaluated on a systematic basis in quasi-static simulations involving DEM.

3.3 Balance of angular momentum

Rearranging the second term of the moment balance condition in equation (3.2), and expressing it in terms of the number of contacts instead of the number of particles, it can be shown that

$$\sum_{\beta=1}^{N_t} \boldsymbol{h}^\beta \times \boldsymbol{t}^\beta + \sum_{\alpha=1}^{N_c} \boldsymbol{d}^\alpha \times \boldsymbol{f}^\alpha = \boldsymbol{0} \tag{3.14}$$

As pointed out by Bardet and Vardoulakis [41], the first term of equation (3.14) is generally nonzero, but its relative significance decreases as the size of the particle system increases. For a large particulate assembly, it is generally negligible. In addition, when uniform regularly packed particles are tested under uniform and symmetric loads, $\sum_{\beta=1}^{N_t} \boldsymbol{h}^\beta \times \boldsymbol{t}^\beta = \boldsymbol{0}$, even for a small number of particles. Under these circumstances,

$$\sum_{\alpha=1}^{N_c} \boldsymbol{d}^\alpha \times \boldsymbol{f}^\alpha = \boldsymbol{0} \tag{3.15}$$

Using the properties of the cross product plus equation (3.8), the homogenized stress is found to be symmetric due to balance of angular momentum, i.e.,

$$\boxed{\bar{\boldsymbol{\sigma}} = \bar{\boldsymbol{\sigma}}^T} \tag{3.16}$$

This equation is an alternative expression of equation (2.7) with respect to the rotation DOFs. As a necessary condition, equation (3.16) itself does not rigorously infer balance of angular momentum. Similar to equation (3.11), however, a systematic monitoring of equation (3.16) in explicit DEM schemes can make it an effective criterion to evaluate the static balance of mo-

ments. Equation (3.11) and equation (3.16) furnish a complete set of criteria to evaluate static equilibrium in quasi-static DEM simulations. These criteria will be used in the subsequent sections to provide a systematic framework for i) assessing quasi-static conditions in DEM simulations and ii) unambiguously performing algorithmic calibration, achieving algorithmic parameters yielding meaningful numerical results.

Remark 2. The conventional homogenized stress $\bar{\boldsymbol{\sigma}}$ is not the only expression to represent the average stress state of a particulate assembly. For instance, Chang and Kuhn [42] derived an average stress that is quite similar to $\bar{\boldsymbol{\sigma}}$ but is generally symmetric. Using equation (3.9), if both sides of equation (3.9) add an identical term so that $\boldsymbol{x}^{\beta}$ refers to the point where the external force $\boldsymbol{f}^{\beta}$ is applied, instead of the particle centroid, then the resulting quantity on the left hand side of equation (3.9) becomes an ideally symmetric stress measure. The interested reader is referred to [42] for a more rigorous derivation and detailed discussion. Note that the idea of using homogenized-stress-based criteria to evaluate quasi-static states in particulate mechanics methods is not limited to the conventional homogenized stress $\bar{\boldsymbol{\sigma}}$. Using the average stress derived by Chang and Kuhn, a set of criteria similar to equations (3.11) and (3.16) can be derived as well, in which the external stress will be modified accordingly.

4 Numerical examples and parametric studies

Now that the criteria for static equilibrium have been determined, the issue of how to perform algorithmic calibration using these criteria can be addressed. Before presenting an optimal procedure for the calibration process, it is worth performing a parametric study to investigate the effect of each major algorithmic parameter on the quality of the numerical solution. Several important purposes are served by such a study. First, it helps explain how to use the proposed criteria to evaluate quasi-static states in a systematic manner. Furthermore, development of a general procedure for the algorithmic calibration relies heavily on understanding the effect of each individual parameter. Finally, the parametric study demonstrates possible consequences resulting from performing algorithmic calibration improperly, which reiterates the significance of the criteria developed herein and the importance of regularizing algorithmic calibrations

for explicit DEM schemes.

4.1 Systematic evaluation of the criteria

As pointed out in Section 3, the two proposed criteria are necessary conditions of static equlibrium. Satisfaction of these criteria at a given time instant does not necessarily infer static equilibrium. For example, a particulate assembly in an oscillating state might satisfy both criteria at a certain time instant. However, if these two criteria are evaluated constantly throughout a loading period (e.g., using a series of monitoring points prescribed at small and uniform time intervals, described herein as 'systematically'), and if satisfaction of these two criteria is constantly confirmed at each monitoring point, then it becomes a 'high-probability-event' that quasi-static equilibrium has been achieved. The systematic monitoring can be easily implemented in DEM codes by recording the homogenized stress $\bar{\sigma}_{ij}$ and the external stress $\bar{e}_{ij}$ periodically. Examples will be shown in the subsequent subsections on how to systematically assess the quasi-static conditions using the proposed criteria.

4.2 Numerical specimen and experiment

The DEM code used in this study adopts the stationary explicit scheme introduced in Section 2.2. Note that algorithmic calibrations need to be performed for both the iterative and the stationary schemes to achieve quasi-static conditions, and both need rigorous criteria to guide the calibrations. The findings of the parametric study presented herein are applicable to iterative schemes as well.

Using the stationary explicit scheme, a series of numerical experiments with various algorithmic parameters have been conducted on regularly-packed particulate assemblies to produce stress-strain responses under plane strain conditions. In all cases, the numerical specimen is composed of a single layer of uniform spherical particles in plane. Figure 5a shows the structure of the regular packing, which is characterized by the parameter α, herein referred to as the packing angle. The numbers of the particles located on the two perpendicular boundaries, N_1 and N_3, designate the size of the assembly. Figure 5b shows the imposed boundary
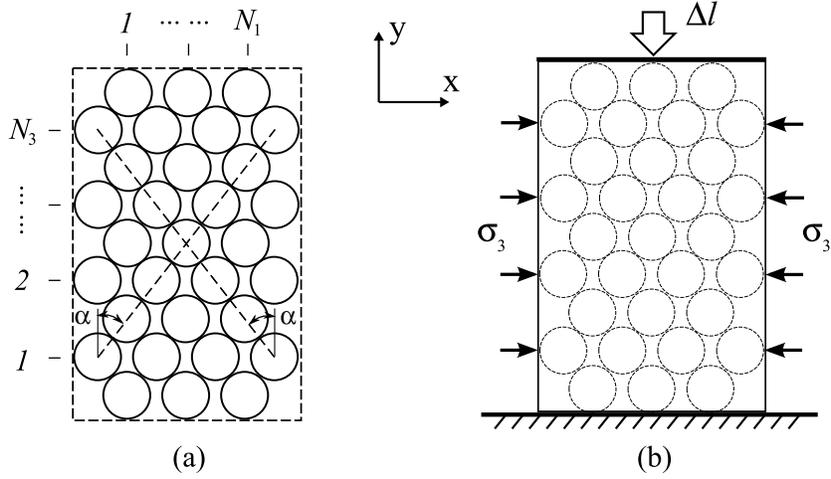
Figure 5: Setup of numerical experiments.

conditions for the experiment, in which the top of the specimen is pushed by a rigid 'platen', moving downwards at a prescribed rate. The lateral confinement is kept constant by imposing constant forces evenly distributed on the particles located on the lateral boundaries.

In this parametric study, the uniform particle diameter is 1.5 mm. The size of the assembly is 10×10, i.e., $N_1 = N_3 = 10$. The structural angle $\alpha = 30°$, corresponds to dense packing. Each particle has the same material properties, with a Young's modulus $E_\mu = 69$ GPa, a Poisson's ratio $\nu_\mu = 0.3$ and an intergranular friction angle $\phi_\mu = 30°$. The material density is $2700\,\mathrm{kg/m^3}$, and gravity is ignored. As a result, the external stress equals the boundary stress, i.e., $\bar{\boldsymbol{b}} = \bar{\boldsymbol{e}}$, cf. equations (3.10) and (3.12). There is no friction on the boundary of the specimen. The total prescribed vertical displacement of the upper 'platen' is 0.05 mm, corresponding to a total vertical strain of 0.18%. Throughout an 'experiment', the equivalent lateral stress $\sigma_3 = 50$ kPa.

One advantage of using regular packing is that an analytical solution exists for the strength of the particulate assembly. Utilizing the condition for sliding at contact points and the symmetry of the packing structure, it can be shown that the maximum stress ratio that can be sustained by the assembly is given by

$$\left.\frac{\sigma_1}{\sigma_3}\right|_{max} = \cot(\alpha - \phi_\mu)\frac{2\cos\alpha + 1/N_3}{2\sin\alpha + 1/N_1} \tag{4.1}$$

19

As N_1 and N_3 grow, equation (4.1) will approach the analytical solution given by Rowe [43]

$$\left.\frac{\sigma_1}{\sigma_3}\right|_{max} = \cot(\alpha - \phi_\mu) \cot \alpha \tag{4.2}$$

For the problem concerned in this parametric study, $\sigma_{1max} = 352\,\text{kPa}$. This value serves as an extra and important measure, in addition to the proposed criteria, to evaluate the results obtained from the 'experiments', which will be discussed subsequently.

4.3 Initial values for calibration

The algorithmic parameters involved in the explicit scheme applied herein include the loading rate, the time step, the fictitious mass and the damping. For simplicity, all particles in the assembly have the same fictitious mass m and the same damping coefficients D_t and D_r corresponding to the translational and rotational DOFs, respectively. As a typical trial-and-error process, the algorithmic calibration of the explicit DEM scheme starts with certain initial values for the algorithmic parameters. Unless a mass scaling method [37] is used, the fictitous mass m typically equals the actual particle mass m_p. For choosing proper initial values for other parameters, there exist a number of guidelines based on previous research.

The upper bound of the time step is limited by the critical time step Δt^crit. For a linear undamped system solved using an explicit scheme, Δt^crit is given by

$$\Delta t^\text{crit} = \frac{2}{\sqrt{\lambda_\text{max}}} \tag{4.3}$$

where λ_max denotes the maximum eigenvalue of the $\boldsymbol{M}^{-1}\boldsymbol{K}$ matrix [34; 44], while the mass matrix $\boldsymbol{M}$ and the stiffness matrix $\boldsymbol{K}$ have been defined in the previous section. Note that equation (4.3) only applies to undamped systems and $\boldsymbol{K}$ is not actually assembled in explicit DEM schemes. Therefore, it is not desirable to use equation (4.3) to estimate the initial value for the time step. For a 1-D generalized mass-spring system, the critical time step is simply given by

$$\Delta t^\text{crit} = 2\sqrt{m_\text{g}/k_\text{g}} \tag{4.4}$$

where m_{g} and k_{g} represent the generalized mass and the generalized spring stiffness, respectively. Equation (4.4) is a common starting point for numerous ad hoc methods for determining an 'effective mass' and 'effective stiffness'. Dependent upon the complexity of the analyzed system and the treatment of damping, such approaches usually necessitate an additional time step reduction parameter so that stable computations can be carried out [18; 36]. As will be shown subsequently, this reduction parameter can be obtained by applying the criteria proposed herein.

To approach the critical time step for a DEM system, m_{g} and k_{g} in equation (4.4) should correspond to their minimum and maximum values, respectively. Note that m_{g} and k_{g} are generalized measures. For a translation DOF system, m_{g} refers to the particle mass m_{p}, while k_{g} is equal to k_{n} defined in equation (2.1). For a rotation DOF system, i.e., a mass allowed to rotate around its centroid, m_{g} represents the moment of inertia of the particle, equal to $2m_{\mathrm{p}}r^2/5$ for spheres with r denoting the particle radius, while $k_{\mathrm{g}} = k_{\mathrm{t}}r^2$ with k_{t} defined in equation (2.3). Let $\Delta t_{\mathrm{t}}^{\mathrm{crit}}$ denote the critical time step computed for translation DOFs and $\Delta t_{\mathrm{r}}^{\mathrm{crit}}$ denote that computed for rotation DOFs. For spherical particles, it can be shown that $\Delta t_{\mathrm{r}}^{\mathrm{crit}} < \Delta t_{\mathrm{t}}^{\mathrm{crit}}$. Therefore,

$$\Delta t^{\mathrm{crit}} = \Delta t_{\mathrm{r}}^{\mathrm{crit}} = 2\sqrt{(2m_{\mathrm{p}})/(5k_{\mathrm{t}})} \tag{4.5}$$

For a nonlinear contact model, like those introduced in Section 2.1, k_{t} depends on the contact displacement δ_{n}. In this study, the maximum stiffness is used to calculate Δt^{crit} by using the maximum value of δ_{n} encountered in a computation.

For a 1-D generalized mass-spring-damper system, a critical damping coefficient exists, which enables the system to return to its balanced state faster than any other damping coefficient and without oscillation. For a translation DOF system, the critical damping is given by

$$D_{\mathrm{t}}^{\mathrm{crit}} = 2\sqrt{m_{\mathrm{p}}k_{\mathrm{n}}} \tag{4.6}$$

21

and for a rotation DOF system,

$$D_{\mathrm{r}}^{\mathrm{crit}} = 2r^2\sqrt{2m_{\mathrm{p}}k_{\mathrm{t}}/5} \tag{4.7}$$

Note that $D_{\mathrm{t}}^{\mathrm{crit}}$ and $D_{\mathrm{r}}^{\mathrm{crit}}$ have different units and apply to the two different DOFs, respectively.

In this study, since the total vertical displacement has been prescribed, the loading rate is represented by the total step number N_{step}. The larger N_{step} is, the lower the loading rate will be. Although there is no rigorously derived critical value available for N_{step}, the parametric study presented herein will provide useful information for choosing an appropriate initial value for N_{step}.

4.4 Benchmark case

Figure 6 plots the homogenized stress and the boundary stress versus vertical strain obtained from a successfully completed calibration. The purpose here is to set up a benchmark case, to which the results from other computations using non-optimal algorithmic parameters can be compared. The calibration procedure will be discussed in the next section. For the vertical components, the $\bar{\sigma}_{\mathrm{yy}}$ curve closely matches the $\bar{b}_{\mathrm{yy}}$ curve, indicating a well-maintained force balance in that direction. Meanwhile, the computed peak vertical stress is close to $352\,\mathrm{kPa}$, the analytical solution, marked by a black arrow in the figure. For the horizontal components, $\bar{\sigma}_{\mathrm{xx}}$ is constantly equal to $50\,\mathrm{kPa}$, the prescribed lateral stress, indicating a horizontal force balance. For the shear stress components, both $\bar{\sigma}_{\mathrm{xy}}$ and $\bar{\sigma}_{\mathrm{yx}}$ are relatively small ($< 1.5\,\mathrm{kPa}$). For an even smaller particle assembly, it has been shown that the shear stress components can be as small as $5 \times 10^{-10}\,\mathrm{kPa}$ under a similar loading condition [45], which generally does not happen in larger systems. In Figure 6, $\bar{\sigma}_{\mathrm{xy}}$ and $\bar{\sigma}_{\mathrm{yx}}$ very closely match one another throughout the simulation, indicating a persistent balance of moments. Hence, the two criteria for static equilibrium are systematically satisfied, which is additionally verified by the match between the computed and the analytical solutions for the peak strength. In conclusion, the quasistatic states have been successfully achieved throughout the computation in this benchmark case.
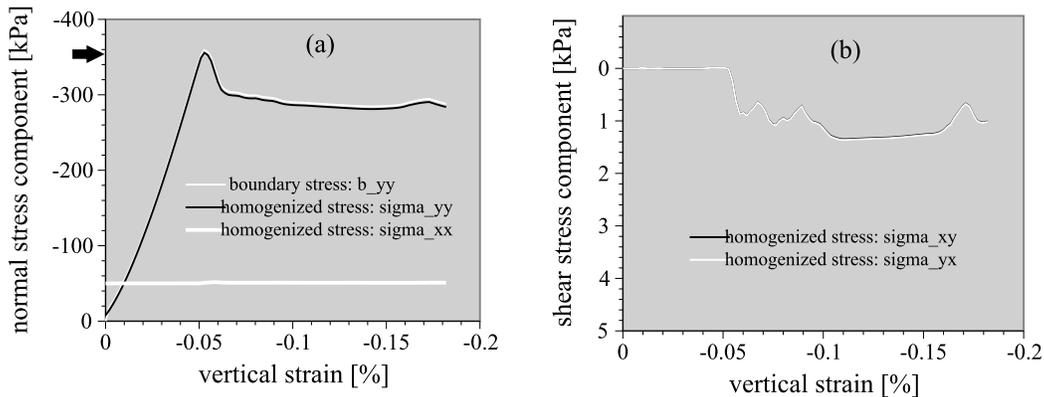
Figure 6: Normal (a) and shear (b) stresses plotted versus vertical strain for the 'benchmark' computation.

The optimized values for the four algorithmic parameters are $\Delta t^{\mathrm{bm}} = 0.2\Delta t^{\mathrm{crit}}$, $D_{\mathrm{t}}^{\mathrm{bm}} = D_{\mathrm{t}}^{\mathrm{crit}}$, $D_{\mathrm{r}}^{\mathrm{bm}} = D_{\mathrm{r}}^{\mathrm{crit}}$ and $N_{\mathrm{step}}^{\mathrm{bm}} = 3 \times 10^5$, where the superscript 'bm' indicates 'benchmark'. Mass scaling has not been used, and therefore the fictitious mass equals the actual particle mass. Note that the data shown in Figure 6 corresponds to 100 monitoring instants evenly spaced throughout the 'experiment'. Compared to the applied N_{step} value, the computation cost due to the systematic monitoring is negligible.

4.5   Loading rate

As mentioned before, the loading rate refers to the magnitude of load or displacement prescribed per unit time step. The loading rate and the time step are two independent algorithmic parameters in explicit schemes. Unlike other algorithmic parameters, the loading rate has not gained much attention in DEM applications. A large loading rate tends to make the computed response dynamic rather than quasi-static. As an extreme case, a large strain, say, of 1%, would result in an unreasonably large contact force if applied to a particulate assembly in just one step. Using the contact model introduced in Section 2.1, extremely large particle velocity will be generated via the motion equations, making the entire computation meaningless. Note that this effect of the loading rate on the computed results applies to both the iterative and the stationary explicit schemes for DEM (cf. Section 2).

23
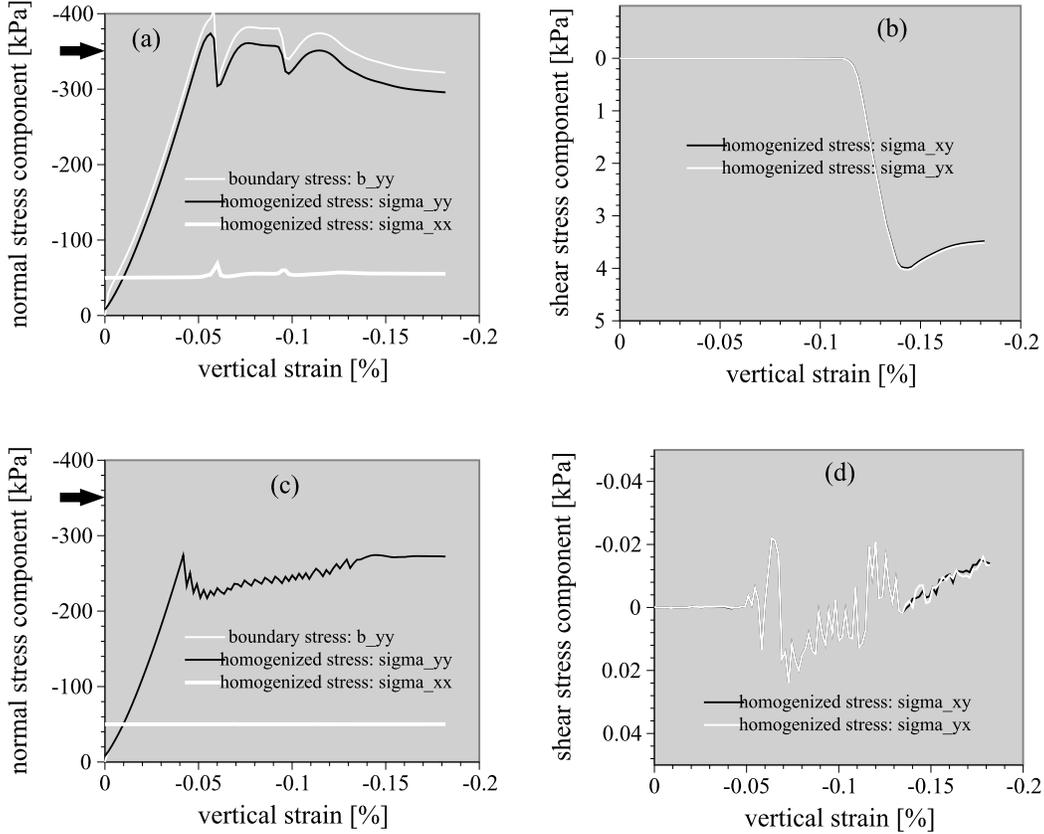
Figure 7: Effect of loading rate (N_{step} varied for a total vertical strain equal to 0.18%). (a) and (b): $N_{\text{step}} = N_{\text{step}}^{\text{bm}}/6 = 5 \times 10^4$; (c) and (d): $N_{\text{step}} = (100/3)N_{\text{step}}^{\text{bm}} = 10^7$

Figures 7a and 7b show a computation using an N_{step} that is one sixth of the $N_{\text{step}}^{\text{bm}}$, with the other parameters equal to their benchmark values. Though $\bar{\sigma}_{\text{xy}}$ mostly matches $\bar{\sigma}_{\text{yx}}$ in Figure 7b, it can be seen from Figure 7a that there is significant gap between $\bar{b}_{\text{yy}}$ and $\bar{\sigma}_{\text{yy}}$, indicating an unbalanced force in the vertical direction. Compared to the analytical solution, the peak strength is overpredicted. Furthermore, the post-peak stress-strain response clearly differs from that observed in the benchmark case. This case verifies that the loading rate has an upper bound (or N_{step} has a lower bound) for the quasi-static regime.

It might not be as straightforward to realize that there exists a lower bound for the loading rate. Figures 7c and 7d show a computation using an N_{step} about 33 times that of $N_{\text{step}}^{\text{bm}}$. In this case, $\bar{\sigma}_{\text{xy}}$ and $\bar{\sigma}_{\text{yx}}$ are closer to zero, which is good. However, the computed strength

of the material is significantly lower than the analytical solution. An interesting observation in Figure 7c is that a zigzag pattern is legible in both the $\bar{b}_{yy}$ and $\bar{\sigma}_{yy}$ curves which mostly coincide with each other. This pattern is different from the noise introduced by transient effects, where $\bar{b}_{yy}$ and $\bar{\sigma}_{yy}$ typically do not match, as will be shown in subsequent cases.

In summary, both upper and lower bounds exist for the loading rate. Thus, Cundall and Strack's suggestion that "the departure from equilibrium may be made as small as desired by reducing the applied loading rate"[1] should be heeded with careful understanding.

4.6   Time step

As discussed in Section 4.3, the time step should not be too large. But this does not necessarily mean that smaller time steps are always better. Figures 8a and 8b show a computation using a Δt that is one tenth of Δt^{bm} with the other parameters equal to their benchmark values. Similar to what was observed in the previous case, a significant gap exists between $\bar{b}_{yy}$ and $\bar{\sigma}_{yy}$. In addition, the strength of the numerical specimen is overpredicted, indicating an unbalanced system and a spurious result. Therefore, there exists a lower bound of Δt for obtaining quasi-static conditions, which should not be confused with the situation of a dynamic DEM application. In the latter case, Δt is only limited by the stability consideration, while smaller time steps always make computed results closer to the exact solution. The bottom line is that the dynamic effect will not be reduced by reducing the time step.

Certainly, the upper bound cannot exceed the critical time step, but how close is it to the critical value? Figures 8c and 8d plot the data from a computation using a Δt that is 1.5 times that of Δt^{bm}, which is 30% of Δt^{crit}. As shown, the peak vertical stress computed is significantly lower than $352\,\text{kPa}$, the analytical solution, and the post-peak behavior is overwhelmed by oscillation. Furthermore, the shear stresses are relatively large and $\bar{\sigma}_{xy}$ is oppositely different from $\bar{\sigma}_{yx}$. All of these observations are indicative of unbalanced forces and moments.

With the other parameters in the neighbourhood of their optimal values, detection of excessive oscillation indicates that the applied time step is too large. If there is a separation
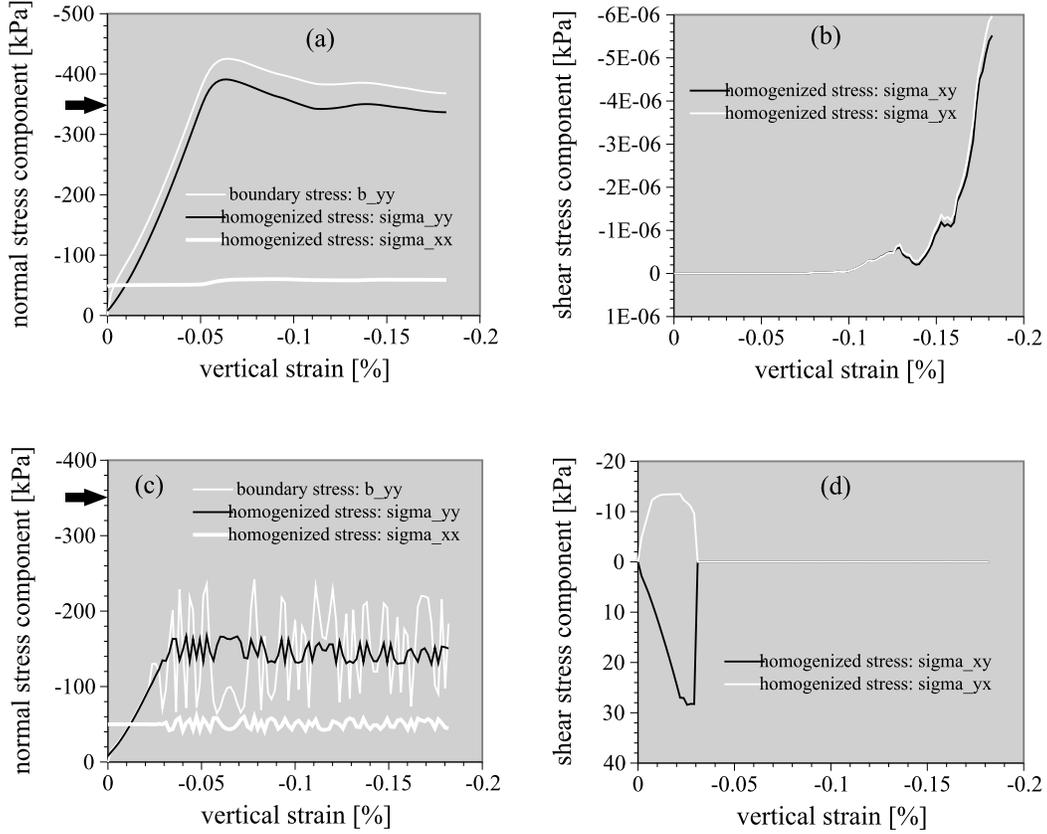
Figure 8: Effect of time step. (a) and (b): $\Delta t = 0.1\Delta t^{\mathrm{bm}} = 0.02\Delta t^{\mathrm{crit}}$; (c) and (d): $\Delta t = 1.5\Delta t^{\mathrm{bm}} = 0.3\Delta t^{\mathrm{crit}}$

of the external stress and the homogenized stress without much oscillation, then the applied time step is probably too small. These signature patterns serve as useful guidelines for the algorithmic calibration. This study indicates that the upper bound of the time step is pretty close to its optimal value, while the lower bound is relatively distant. The value optimized in the benchmark case ($\Delta t = 0.2\Delta t^{\mathrm{crit}}$) basically confirms that the optimal value is a fraction of the critical time step [18; 36; 46]. This fraction is case-dependent and generally needs to be determined through algorithmic calibration.

4.7 Damping coefficients

As explained in Section 4.3, the translational damping D_{t} is used for translation DOFs, and the rotational damping D_{r} is used for rotation DOFs. The effects of both types are investigated

26

herein.
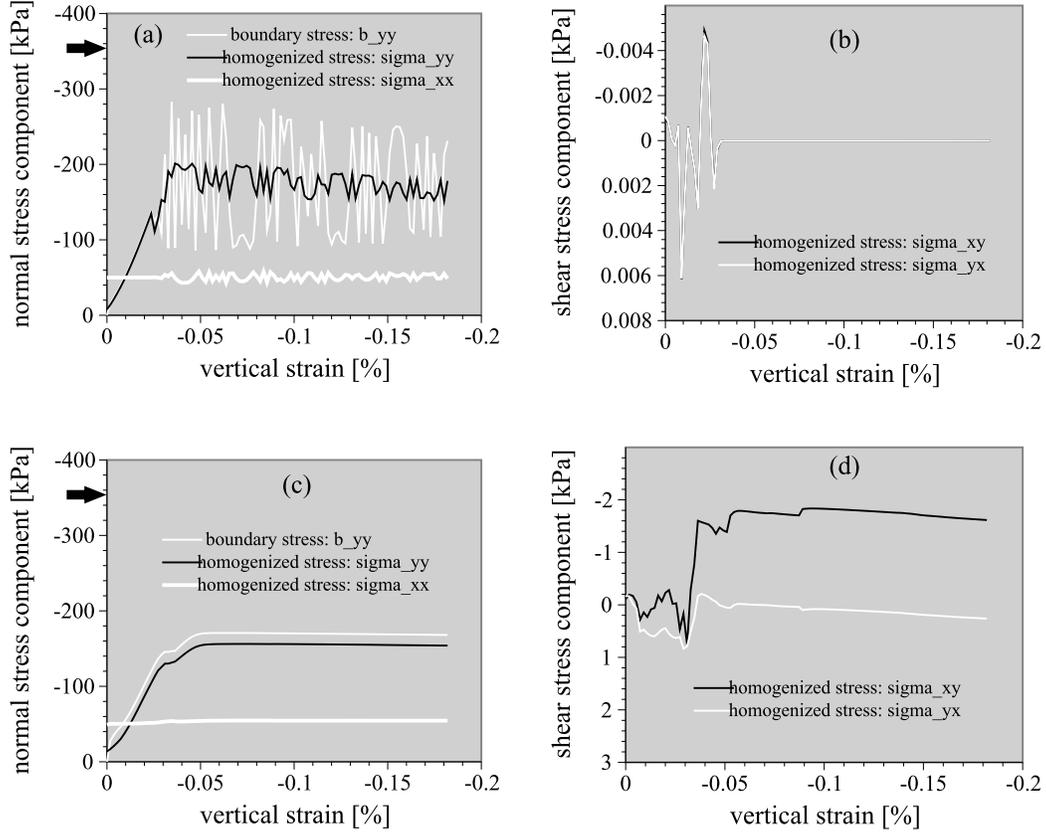
Figure 9: Effect of translational damping. (a) and (b): $D_t = 0.7D_t^{bm} = 0.7D_t^{crit}$; (c) and (d): $D_t = 4.3D_t^{bm} = 4.3D_t^{crit}$

Figures 9a and 9b show a computation using a D_t slightly less than D_t^{bm}, and other parameters equal to their benchmark values. As expected, kinetic energy cannot be effectively absorbed by damping that is too small. Consequently, significant noise is found in the stress-strain curves plotted in Figure 9a, and the computed strength is much lower than the theoretical value. These observations are similar to those made in Figure 8a, but the responses in the shear stress components in the two figures are quite different. Herein, $\bar{\sigma}_{xy}$ and $\bar{\sigma}_{yx}$ are small and identical, indicating a well-maintained moment balance. In algorithmic calibrations, therefore, collective patterns of out-of-bound states could provide informative hints about which parameters should be adjusted next to satisfy the equilibrium criteria.

Figures 9c and 9d show a computation using a D_t that is 4.3 times its benchmark value. In this case, the computed strength of the material is underpredicted, the post-peak response incorrectly exhibits perfect plasticity, and there is a noticeable gap between $\bar{b}_{yy}$ and $\bar{\sigma}_{yy}$. There is no oscillation for this case, which distinguishes it from some previous cases. Furthermore, the shear stress components show that moment balance is not achieved. Note that the operational range of the translational damping coefficient is relatively narrow and that the lower bound is quite close to the optimal value that is equal to the critical translational damping for this 'experiment'.
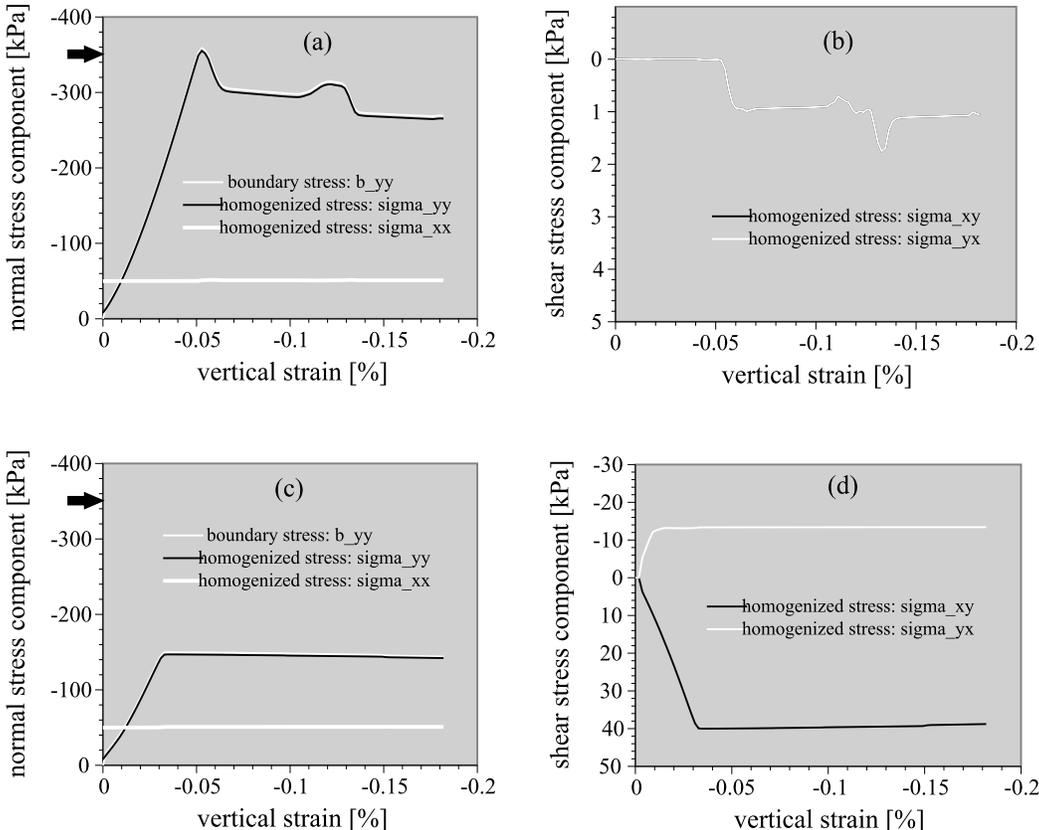
Figure 10: Effect of rotational damping. (a) and (b): $D_r = 0$; (c) and (d): $D_r = 2D_r^{bm} = 2D_r^{crit}$

The rotational damping D_r is another parameter that has been mostly ignored in previous studies. Figures 10a and 10b show a computation using a D_r of zero (i.e., rotational damping

is ignored). As shown, $\bar{b}_{yy}$ matches $\bar{\sigma}_{yy}$ while $\bar{\sigma}_{xy}$ and $\bar{\sigma}_{yx}$ are on top of each other. Compared to the benchmark case, the only noticeable difference is a bump in the post-peak response in Figure 10a. Otherwise, this case seems to be another good example of quasi-static states successfully achieved in the numerical experiment. The slight difference in the post-peak stress-strain response might appear to be trivial, but it can be potentially significant, depending on the purpose of the DEM analysis. Corresponding to the same prescribed vertical strain, Figures 11a and 11b show snapshots of the particle assembly in the benchmark case and the zero rotational damping case, respectively, wherein shear banding has developed as a result of the vertical compression. It can be seen that the shear band in the former case is one particle wider than that in the latter case, which is significant considering the magnitude of the band width. It has been found that the band width in the former case grows as the compression persists, whereas the band width in the latter case does not. Generally speaking, D_r is used to reduce the rotation kinetic energy and previous research has shown that the particle rotation plays a critical role in shear band development [3; 47]. It can be expected that rotational damping will be important in cases where particles tend to be rotated (e.g., in pure shear tests, or when significant tangential forces are applied to the boundaries of a particulate assembly).

(a)   (b)
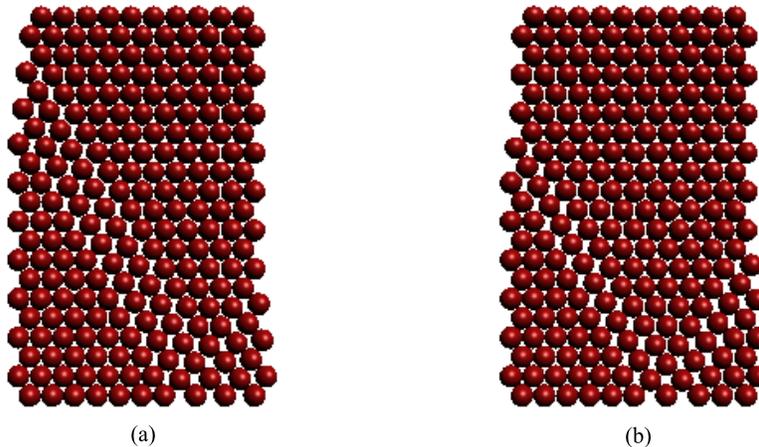
Figure 11: Snapshots of shear banding in plane strain developed in particle assemblies at 2.2% vertical strain, using (a) benchmark values; and (b) $D_r = 0$

Figures 10c and 10d show a computation using a D_r that is two times D_r^{bm}. The most striking observation is the significant moment imbalance, evaluated by the second criterion for static equilibrium. Furthermore, the computed strength of the material is significantly underpredicted, most likely due to the presence of a large moment imbalance in the system. Therefore, an upper bound exists for D_r.

Remark 3. According to the terminology used by Cundall and Strack [1], the damping discussed herein is *global damping*. Alternatively, one can use *contact damping* for dynamic relaxation, which also needs to be calibrated against the equilibrium criteria to achieve quasistatic states.

4.8 Mass scaling

The idea behind mass scaling is simple. Under the same loading conditions, a heavier mass will result in a less significant dynamic effect. Accordingly, the fictitious mass m can be upscaled by

$$m_s = f_{ms} m \tag{4.8}$$

where f_{ms} is the mass scaling factor and m_s is the upscaled mass. Recall that m is a generalized expression. Therefore, f_{ms} applies to both the measure of mass for translation DOFs and the moment of inertia for rotation DOFs. In practice, the mass scaling method is typically used without numerical damping. In this case, only one parameter, f_{ms}, needs to be calibrated.

Figures 12a and 12b show a computation using mass scaling, wherein $f_{ms} = 10^4$, $D_t = D_r = 0$, $\Delta t = \Delta t^{bm}$ and $N_{step} = N_{step}^{bm}$. It can be seen that $\bar{b}_{ij}$ roughly matches $\bar{\sigma}_{ij}$ for each component and $\bar{\sigma}_{xy} = \bar{\sigma}_{yx}$. The peak vertical stress $\bar{\sigma}_{yy}$ is slightly overpredicted, compared to the analytical solution. However, the computed post-peak response herein is apparently different from its counterpart computed in the benchmark case.

In practice, it is common to use a f_{ms} greater than 10^{10} for static DEM analysis. Figures 12c and 12d show a similar computation using $f_{ms} = 10^8$ with all other parameters the same as those used in Figures 12a and 12b. Although moment balance is successfully achieved, balance of force is entirely lost by using such large upscaled masses. The normal
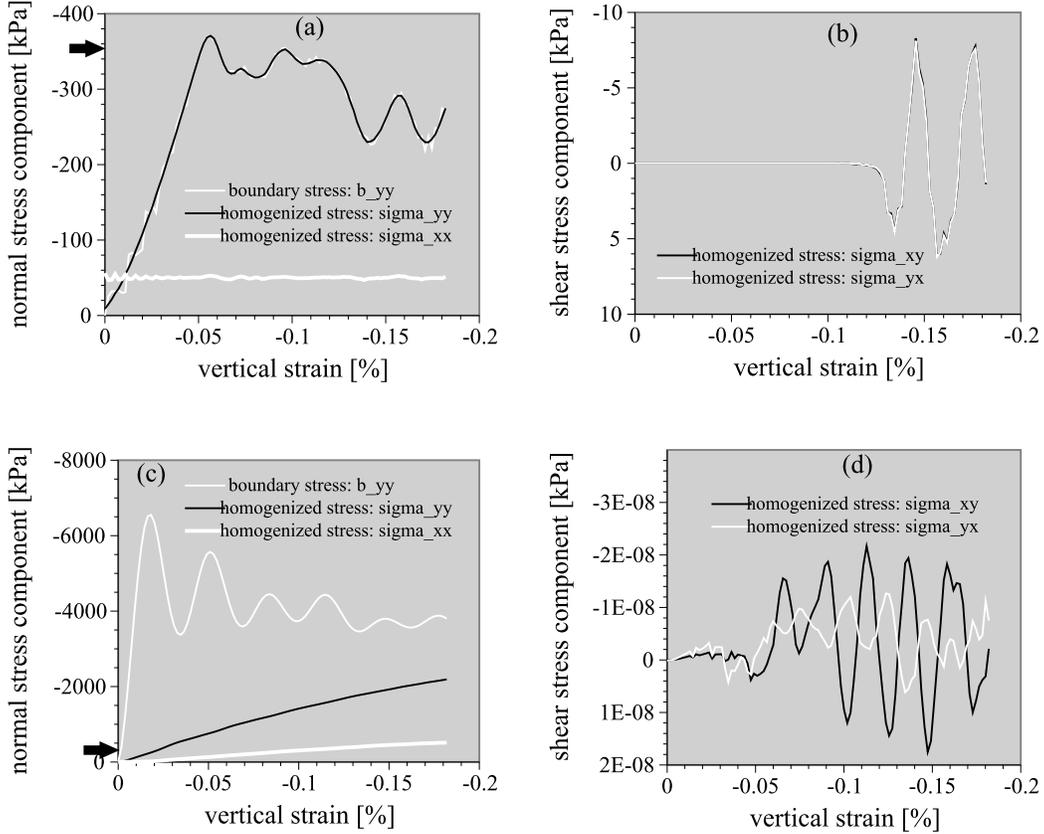
Figure 12: Effect of mass scaling factor. (a) and (b): $f_{\mathrm{ms}} = 10^4$; (c) and (d): $f_{\mathrm{ms}} = 10^8$

components become unrealistically large while the boundary and the homogenized stresses follow two completely different trends. The results would be worse still if an even larger f_{ms} were used.

This parametric study implies that the mass scaling method is not ideally effective in helping an explicit DEM computation obtain quasi-static solutions. Furthermore, setting f_{ms} equal to an arbitrary large number tends to yield unrealistic results distant from the quasi-static state.

5   General procedure for algorithmic calibration

The examples discussed in Section 4 show that the systematic evaluation of the proposed criteria can effectively aid in the algorithmic calibration for explicit DEM schemes to converge

to quasi-static solutions. It is clear that if algorithmic calibration is ignored, or if it is not guided by rigorous criteria, then a spurious result is likely, no matter how realistic the material parameters may be.

The previous section analyzed many deviations from the benchmark case in which the algorithmic parameters were well calibrated; however, the calibration of the benchmark case has not been discussed yet. This section will cover this important topic and provide general guidelines for conducting an algorithmic calibration.

5.1   Effect of assembly size

Most particulate mechanics analyses performed in practice involve a large number of particles and thus demand a considerable amount of computation time. Performing algorithmic calibrations for large scale computations may be extremely inconvenient and prohibitively time-consuming. Thus, the question arises: is it possible to conduct the calibration on a similar but smaller computation?
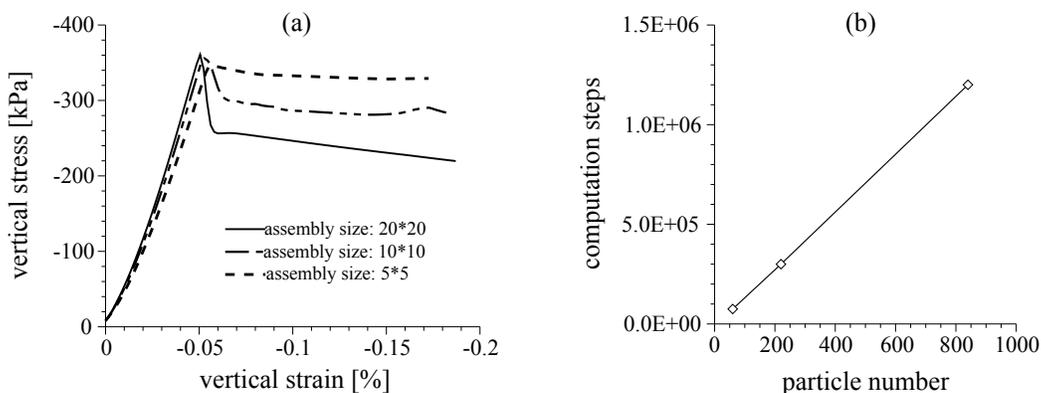
Figure 13: Size effect. (a) stress-strain curve; (b) linear relation between total number of computation steps (N_{step}) and total number of particles (N_p) for same applied strain

To answer this question, three different numerical specimens, of sizes 5×5, 10×10 and 20×20, were numerically tested. The packing structure of these specimens and the testing conditions are shown in Figure 5. These three computations each used the same material properties and the same loading conditions, which included a specified lateral stress and a prescribed total vertical strain. Basically, the 10×10 case is identical to the benchmark case

32

shown in Figure 6 and the other two cases differ from it only by the assembly size. Algorithmic calibration without mass scaling was performed for each case, with the goal of determining whether certain relations exist between the optimized parameters obtained for each case.

Figure 13a plots the vertical homogenized stress versus the vertical strain after the completion of calibration for each case. Basically, the material response was found to be size-dependent, especially in the postpeak stage. Therefore, large DEM analyses cannot be simply replaced by smaller ones, even when the material properties and loading conditions are identical.

However, for the purpose of algorithmic calibration, it has been found that most of the optimal parameters, obtained through calibrations against the equilibrium criteria, are independent of the assembly size. In this study, it was found that $\Delta t = 0.2 \Delta t^{\mathrm{crit}}$, $D_{\mathrm{t}} = D_{\mathrm{t}}^{\mathrm{crit}}$ and $D_{\mathrm{r}} = D_{\mathrm{r}}^{\mathrm{crit}}$ for each of the three assemblies. The only parameter that differed between the assembly sizes was the step number N_{step} which basically represents the loading rate, as mentioned previously. Figure 13b shows that there exists a linear relation between the optimized N_{step} and the total number of particles contained in the assembly. Note that the optimal N_{step} value shown in this figure correspond to the same verticle strain applied, i.e., 0.18%. This result is important because it suggests that the algorithmic calibration does not have to be conducted on the prototypical particulate assembly. Instead, it can be carried out on an assembly 'similar' to the prototype, but smaller in size, as long as the prototypical assembly is macroscopically uniform. In fact, the concept of the so-called representative elementary volume (REV) [48] serves as a good guidance in terms of how to choose the size of the small sample for the calibration purpose.

5.2   Guidelines

Based on the parametric studies presented previously, a general procedure for algorithmic calibration of explicit DEM schemes is suggested as follows.

First, a reasonable assembly size needs to be chosen. For a large particulate assembly to be analyzed, one can 'cut' a REV 'sample' from the prototype to calibrate the algorthmic

parameters involved. Analogous to a typical sample for material testing, the REV sample should be large enough to be representative of the prototypical material, but still small enough to be economical in terms of computational time cost.

Then, the magnitude of the prescribed stress or strain needs to be adjusted. Based on the results shown in Section 4, the signature patterns of out-of-bound parameters mostly manifest themselves in the inelastic regime. Within the elastic range, those signature patterns are generally absent, which makes the proposed criteria hard to evaluate. Thus, the prescribed boundary conditions need to be proportionally magnified if the demonstration of signature patterns is limited.

Next, the parameters are calibrated by trial and error until the two proposed criteria are satisfied in a systematic manner. To ensure a systematic satisfaction of the criteria, both the homogenized stress and the external stress should be constantly monitored throughout the computation. The total number of monitoring points may be as small as desired, as long as the signature patterns of an out-of-bound parameter can be effectively demonstrated.

In terms of initial values, it is recommended to use $\Delta t = 0.2\Delta t^{\text{crit}}$, $D_{\text{t}} = D_{\text{t}}^{\text{crit}}$ and $D_{\text{r}} = D_{\text{r}}^{\text{crit}}$. Generally, N_{step} depends on the loading mode and the loading magnitude. Typically, the critical values for the damping coefficients are close to the optimal values; so, the task boils down to the heuristic calibration of Δt and N_{step}. The signature patterns shown in the corresponding cases in Section 4 serve as a compass for calibrating these two parameters, which is not too difficult for a reasonably sized 'sample'.

Finally, the algorithmic parameters for the prototypical system are projected from the optimized values obtained for the RVE 'sample'. The number of steps N_{step} is linearly upscaled according to the size of the sample and the size of the prototype system, and the other parameters are expected to remain equal.

6   Concluding remarks

In practice, explicit schemes are preferred for solving static problems using DEM. These explicit schemes typically employ a set of motion equations with damping to update particle dis-

placements, essentially following a dynamic relaxation method. Unlike the Newton-Raphson method, the stability of an explicit method is conditional and its convergence to quasi-static solutions depends on the algorithmic parameters involved. The variations and uncertainties encountered in particulate systems make it difficult for the available algorithms to automatically update algorithmic parameters under general conditions. To enable an explicit DEM scheme to converge to quasi-static states, algorithmic calibration is generally required to find the optimal parameter values. To this end, it is important to use appropriate criteria when evaluating quasi-static states of an arbitrary granular system, and also, to set up a procedure to perform the algorithmic calibration in an effective and efficient manner.

In this paper, we have presented two criteria for static equilibrium evaluation in particulate mechanics computations. The first criterion (i.e., the equality between the homogenized stress and the external stress) evaluates balance of forces, while the second criterion (i.e., the symmetry of the homogenized stress) evaluates balance of moments. We have shown that systematically satisfying these two criteria essentially implies that the explicit scheme successfully yields quasi-static solutions. These criteria are based on the homogenized stress derived from sound mathematical and mechanical theories, independent of the size of the particulate assembly and easy to evaluate in particulate mechanics computations (e.g., DEM simulations). With the proposed criteria, algorithmic calibration of explicit DEM schemes can be carried out in a rigorous manner, and quasi-static solutions can be obtained with confidence for arbitrary granular systems.

A series of parametric studies have been performed to investigate the effect of individual algorithmic parameters on the solution computed by the explicit DEM scheme. Signature patterns of each parameter in out-of-bound states were investigated, shedding light on the calibration of these parameters under general conditions. Meanwhile, consequences due to improper algorithmic parameters were also demonstrated, which reiterates the significance of the proposed criteria and the importance of proper algorithmic calibration to the success of the explicit schemes. For simulations of large granular systems, we have shown that it is possible to perform algorithmic calibration in a timely fashion with a minimized computation

cost.

The proposed framework promises to ameliorate the uncertainties and potential challenges associated with the algorithmic calibration and use of explicit DEM methods to model quasi-static problems.

Acknowledgments

References

[1] P. A. Cundall and O. D. L. Strack. A discrete numerical model for granular assemblies. *Géotechnique*, 29:47–65, 1979.

[2] B. Cambou. *Behaviour of Granular Materials*. Springer, New York, NY, 1998.

[3] M. Oda and K. Iwashita. *Mechanics of Granular Materials: An Introduction*. A.A. Balkema, Brookfield, VT, 1999.

[4] R. E. Barbosa-Carrillo. *Discrete Element Models for Granular Materials and Rock Masses*. PhD thesis, University of Illinois, Urbana-Champaign, IL, 1990.

[5] Z. You. *Development of a Micromechanical Modeling Approach to Predict Asphalt Mixture Stiffness Using the Discrete Element Method*. PhD thesis, University of Illinois, Urbana-Champaign, IL, 2003.

[6] F. A. Tavarez. *Discrete Element Method for Modeling Solid and Particulate Materials*. PhD thesis, University of Wisconsin, Madison, CA, 2005.

[7] A. Anandarajah. Multiple time-stepping scheme for the discrete element analysis of colloidal particles. *Powder Technology*, 106:132–141, 1999.

[8] N. G. Deen, M. Van Sint Annaland, M. A. Van der Hoef, and J. A. M. Kuipers. Review of discrete particle modeling of fluidized beds. *Chemical Engineering Science*, 62:28–44, 2007.

[9] Y. Sheng, C. J. Lawrence, B. J. Briscoe, and C. Thornton. Numerical studies of uniaxial powder compaction process by 3D DEM. *Engineering Computations*, 21(2-4), 2004.

[10] B. Severson. *A Nano to Macro Study of Friction and Adhesion in Granular Materials*. PhD thesis, Northwestern University, Evanston, IL, 2007.

[11] P. A. Cundall. Formulation of a three-dimensional distinct element model. I: A scheme to detect and represent contacts in a system composed of many polyhedral blocks. *International Journal of Rock Mechanics and Mining Sciences*, 25(3):107–116, 1988.

[12] X. Lin and T. T. Ng. A three-dimensional discrete element model using arrays of ellipsoids. *Géotechnique*, 47:319–329, 1997.

[13] A. M. Sallam. *Studies on Modeling Angular Soil Particles Using the Discrete Element Method*. PhD thesis, University of South Florida, Tampa, FL, 2004.

[14] F. A. Tavarez and M. E. Plesha. Discrete element method for modelling solid and particulate materials. *International Journal for Numerical Methods in Engineering*, 70:379–404, 2007.

[15] R. I. Borja and J. R. Wren. Micromechanics of granular media, Part I: Generation of overall constitutive equation for assemblies of circular disks. *Computer Methods in Applied Mechanics and Engineering*, 127:13–36, 1995.

[16] C. Wellmann, C. Lillie, and P. Wriggers. Homogenization of granular material modeled by a three-dimensional discrete element method. *Computers & Geotechnics*, 2007. In press.

[17] J. P. Bardet and J. Proubet. A numerical investigation of the structure of persistent shear bands in granular media. *Géotechnique*, 41:599–613, 1991.

[18] T. T. Ng. Input parameters of discrete element methods. *Journal of Engineering Mechanics*, 132:723–729, 2006.

[19] P. A. Cundall. A discontinuous future for numerical modelling in geomechanics? *Geotechnical Engineering, ICE*, 149:41–47, 2001.

[20] C. Miehe and J. Dettmar. A framework for micro-macro transitions in periodic particle aggregates of granular materials. *Computer Methods in Applied Mechanics and Engineering*, 193:225–256, 2004.

[21] A. Munjiza. *The Combined Finite-Discrete Element Method*. Wiley, Hoboken, NJ, 2004.

[22] P. Underwood. Dynamic relaxation. In T. Belytschko and T.J.R. Hughes, editors, *Computational Methods for Transient Analysis*, volume 1, pages 245–265, New York, NY, 1983. Elsevier.

[23] S. P. Timoshenko. *History of Strength of Materials*. McGraw-Hill, New York, 1953.

[24] A. C. Cassell and R. E. Hobbs. Numerical stability of dynamic relaxation analysis of nonlinear structures. *International Journal for Numerical Methods in Engineering*, 10:1407–1410, 1976.

[25] S. W. Key, C. M. Stone, and R. D. Kreig. Dynamic relaxation applied to the quasi-static large deformation inelastic response of axisymmetric solids. In W. Wunderlich, E. Stein, and K.J. Bathe, editors, *Nonlinear Finite Element Analysis in Structural Mechanics*, pages 585–621. Springer, 1981.

[26] K. C. Park. A family of solution algorithms for nonlinear structural analysis based on relaxation equations. *International Journal for Numerical Methods in Engineering*, 18:1337–1347, 1982.

[27] M. Papadrakakis. A method for the automatic evaluation of the dynamic relaxation parameters. *Computer Methods in Applied Mechanics and Engineering*, 25:35–48, 1981.

[28] L. Zhang, M. Kadkhodayan, and Y. W. Mai. Development of the maDR method. *Computers & Structures*, 52:1–8, 1994.

[29] J.P. Bardet and J. Proubet. Adaptive dynamic relaxation for statics of granular materials. *Computers & Structures*, 39:221–229, 1991.

[30] J. Christoffersen, M. M. Mehrabadi, and S. Nemat-Nasser. A micromechanical description of granular material behavior. *Journal of Applied Mechanics*, 48:339–344, 1981.

[31] K. L. Johnson. *Contact Mechanics*. Cambridge University Press, Cambridge, UK, 1985.

[32] R. D. Mindlin and H. Deresiewicz. Elastic spheres in contact under varying oblique forces. *Transactions of ASME, Series E. Journal of Applied Mechanics*, 20:327–344, 1953.

[33] S. van Baars. *Discrete Element Analysis of Granular Materials*. PhD thesis, Delft University of Technology, Delft, Netherlands, 1996.

[34] T. Belytschko, W. K. Liu, and B. Moran. *Nonlinear Finite Elements for Continua and Structures*. John Wiley & Sons Ltd., West Sussex, UK, 2000.

[35] T. J. R. Hughes. *The Finite Element Method*. Prentice-Hall, Englewood Cliffs, NJ, 1987.

[36] C. O'Sullivan and J. D. Bray. Selecting a suitable time step for discrete element simulations that use the central difference time integration scheme. *Engineering Computations*, 21:278–303, 2004.

[37] C. Thornton. Numerical simulations of deviatoric shear deformation of granular media. *Géotechnique*, 50(1):43–53, 2000.

[38] A. Drescher and G. de Josselin de Jong. Photoelastic verification of a mechanical model for the flow of a granular material. *Journal of the Mechanics and Physics of Solids*, 20:337–351, 1972.

[39] J. Goddard. An elastohydrodynamics theory for the rheology of concentrated suspensions of deformable particles. *Journal of Non-Newtonian Fluid Mechanics*, 2:169–189, 1977.

[40] L. Rothenburg and A. P. S. Selvadurai. A micromechanical definition of the cauchy stress tensor for particulate media. In A. P. S. Selvadurai, editor, *Mechanics of Structured Media*, pages 469–486, Amsterdam, 1981. Elsevier.

[41] J. P. Bardet and I. Vardoulakis. The asymmetry of stress in granular media. *International Journal of Solids and Structures*, 38:353–367, 2001.

[42] C. S. Chang and M. R. Kuhn. On virtual work and stress in granular media. *International Journal of Solids and Structures*, 42:3773–3793, 2005.

[43] P. W. Rowe. The stress-dilatancy relation for static equilibrium of an assembly of particles in contact. *Proceedings of the Royal Society of London, Series A*, 269:500–527, 1962.

[44] T. Belytschko and T. J. R. Hughes. *Computational Methods for Transient Analysis*, volume 1 of *Computational Methods in Mechanics Series*. North-Holland, New York, NY, 1983.

[45] X. Tu and J. E. Andrade. Criteria for static equilibrium in discrete element method. 2007. ASME 2007 International Mechanical Engineering Congress Exposition. In CD.

[46] Itasca Consulting Group. *PFC2D Particle Flow Code in Two Dimensions*. Itasca Consulting Group, Minneapolis, 1998.

[47] J. P. Bardet. Observations on the effects of particle rotations on the failure of idealized granular materials. *Mechanics of Materials*, 18:159–182, 1994.

[48] S. Nemat-Nasser and M. Hori. *Micromechanics: Overall Properties of heterogeneous Materials*. Elsevier Science Publisher, Amsterdam, 1993.